A Compact Q-Band Rectangular Waveguide Thermal Isolator

Giorgio Montisci, *Senior Member, IEEE*, Giuseppe Valente, Giacomo Muntoni, Pasqualino Marongiu, and Tonino Pisanu

***Abstract*— We present a new waveguide thermal isolator, based on a simple gap in a standard rectangular waveguide, developed for the Q-band cryogenic receiver of the Sardinia Radio Telescope. The proposed component is very compact and consists of a single module, including both the horizontal and vertical polarization channels and the noise injection channel. The electromagnetic and thermal characteristics of this isolator have been fully investigated. High return loss and low insertion loss are obtained solely by a proper selection of the waveguide wall thickness, thus resulting in a very simple design, easily scalable in the whole microwave range. High robustness to misalignment and excellent thermal performance are achieved. A prototype of the proposed isolator has been manufactured and tested at room temperature, showing a very good agreement with predicted performance.**

***Index Terms*— Cryogenics, Q-band, radio astronomy, rectangular waveguide, Sardinia Radio Telescope (SRT), thermal isolator.**

I. Introduction

MODERN radio frequency (RF) receivers for astronomy and space applications are designed to operate at cryogenic temperature in order to increase the system sensitivity by reducing the thermal noise [1]–[3]. However, the microwave components employed in the receiver chain, such as feed horns, orthomode transducers, directional couplers, filters, amplifiers, waveguide sections, and cables, employ excellent electric conductors that are also excellent heat conductors and, therefore, provide a very low thermal resistance between the external environment (at room temperature) and the microwave devices cooled at cryogenic temperatures (usually ∼70 or ∼20 K). A direct low loss metallic connection between parts operating at very different temperatures requires power consumption to maintain the operating temperature of the cooled devices. This drawback can be avoided by using thermal gaps in waveguide structures, supported by proper insulating materials [4]–[7].

A gap in a waveguide allows increasing the thermal resistance but calls for an accurate mechanical and electromagnetic design and should provide low insertion loss (IL) and high return loss (RL) over the receiver bandwidth while minimizing the thermal power required to maintain the cryogenic operating temperature. Moreover, since the components at cryogenic temperature are housed inside a cryostat, they should be as small as possible.

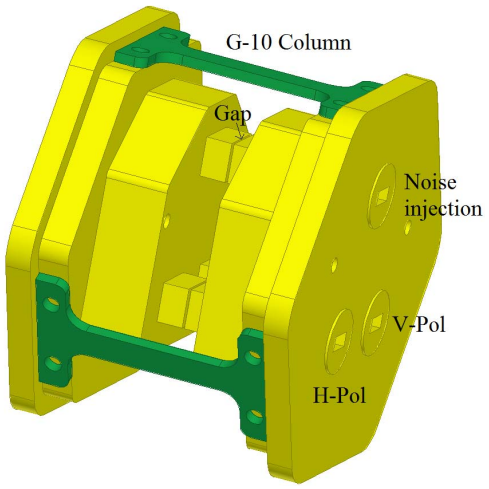

Fig. 1. 3-D model of the proposed thermal isolator.

In this article, a new rectangular waveguide-based thermal isolator has been designed and thoroughly characterized from the electromagnetic, mechanical, and thermal points of view, aiming to meet the specifications of the Q-band receiver of the Sardinia Radio Telescope (SRT) [8]–[11].

The Q-band multifeed receiver of the SRT will be composed of 19 separate receiver chains, each one including the horizontal and vertical polarization channels, and a third channel for the injection of a noise source for calibration purposes [12], [13]. Consequently, three thermal gaps are required for each of the 19 receiver chains. In order to save space (and refrigerating power), these three gaps have been integrated into a single module (see Fig. 1). Each channel of this module is realized using standard WR22 rectangular waveguides, and the thermal isolation is ensured using a gap between two waveguide sections. G-10 fiberglass-epoxy [14] flat columns are used to support the waveguide flanges and to determine the waveguide gaps of each module (Fig. 1).

The first step in the design of the gap between two waveguide sections has been the analysis of the performance of the standard choke flange [15], which is indeed designed to compensate for imperfect mating and small gaps between the flanges. From ANSYS HFSS simulations, we have found

Manuscript received July 16, 2019; revised October 16, 2019; accepted October 18, 2019. Date of publication December 4, 2019; date of current version January 31, 2020. *(Corresponding author: Giorgio Montisci.)*

G. Montisci and G. Muntoni are with the Dipartimento di Ingegneria Elettrica ed Elettronica, Università degli Studi di Cagliari, 09123 Cagliari, Italy (e-mail: giorgio.montisci@.unica.it).

G. Valente is with the Italian Space Agency, 00133 Rome, Italy (e-mail: giuseppe.valente@asi.it).

P. Marongiu and T. Pisanu are with the National Institute for Astrophysics (INAF), Cagliari Astronomy Observatory, 09047 Cagliari, Italy (e-mail: pasqualino.marongiu@inaf.it; tonino.pisanu@inaf.it).

Color versions of one or more of the figures in this article are available online at http://ieeexplore.ieee.org.

Digital Object Identifier 10.1109/TMTT.2019.2950662

that this solution allows obtaining good performance over the Q-band (RL better than 30 dB for a gap of 100 μm between the waveguide flanges). However, this is true only when the two flanges are perfectly aligned, whereas even a small misalignment reduces the performance, generating undesired in-band spikes, which makes the standard choke flange not suitable for the realization of waveguide thermal gaps covering the entire Q-band.

Given the results of the thermal gap implemented with a choke flange configuration, we expect that also a simple gap realized by facing two separate WR22 waveguide sections is not able to guarantee the required performance over the Q-band. In fact, also in this latter case, the frequency response exhibits in-band resonances, which appear as undesired transmission minima. However, we have found that these resonances, generated by the power radiated through the gap, depend on the thickness of the waveguide wall. Therefore, the waveguide wall thickness has been used as the only design parameter, and it is adjusted to move the undesired resonances outside the operating band.

The proposed design is very simple, compact, provides high electromagnetic and thermal performance, with a measured RL better than 30 dB in case of aligned flanges, and an excellent robustness even to a substantial misalignment of the two waveguide flanges (measured RL better than 26 dB). It has been developed mainly taking into account the following.

1) The design of the cryostat is constrained by the limited space available in the direction of the optical axis inside the focal cabin of the SRT, thus requiring a compact realization.
2) The maximum power required to maintain the cryogenic temperature of 20 K is set to 150 mW (for each of the 19 channels) by the specifications of the whole receiver system.

These constraints, although intended for the multifeed Q-band receiver of the SRT, are desirable for a generic cryogenic receiving system. Therefore, the proposed solution will not be limited to this specific application.

To the best of our knowledge, few thermal isolators can be found in the literature and none of them is able to provide both a compact realization, with the required thermal isolation, and an RL better than 25 dB over the operating frequency range (41% bandwidth in our case).

In [4], a *Ka*-band waveguide thermal isolator is proposed, but a large insulating foam structure is used to encase the waveguides. This structure could be scaled in the Q-band using WR22 waveguides but would occupy too much space inside the cryostat. Moreover, the electromagnetic performance of this isolator is not satisfactory, providing a large IL (up to 1 dB at the edge of the bandwidth) and a poor RL.

In [5], a W-band thermal isolator is based on a microwave bandgap joint. This structure is immune to misalignment, the IL of the measured prototype is less than 0.4 dB, and the RL is better than 20 dB over the operating band in the case of aligned flanges. However, this configuration should be reengineered to include three separate channels in a single module, and it generates undesired ripples in the measured RL, which is up to 5 dB worse than the simulated one. Moreover, measured results are not provided for misaligned flanges.

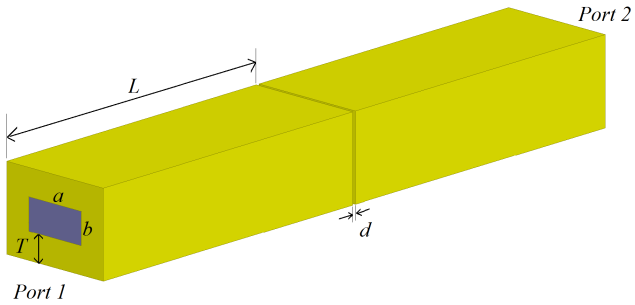

Fig. 2. Gap in a WR22 waveguide.

Another solution [6] employs dielectric waveguides to self-sustain the waveguide gap but providing unsatisfactory IL and RL for high-performance RF receivers. The simulated 20-dB RL bandwidth is about 27% and the measured results of a waveguide-microstrip converter, which employs two thermal isolators, show an RL of 14 dB over a bandwidth of only 21%. Moreover, the solution proposed in [6] reduces the transverse waveguide dimension, which is useful in the lower part of the microwave range but could be unnecessary at millimeter wavelengths. On the other hand, using dielectric-filled waveguides requires matching the thermal gap to the components of the receiving chain connected to it, which are usually realized using standard air-filled waveguides to reduce losses (as in our case).

A simplified two-channel prototype of the proposed isolator has been manufactured and tested at room temperature, showing a very good agreement with predicted performance.

II. Electromagnetic Design of the Thermal Isolator

A. Design and Characterization of the Single-Channel Waveguide Thermal Isolator

A WR22 waveguide configuration has been selected to achieve the thermal isolation over the Q-band (33–50 GHz). The dimensions of the standard WR22 waveguide are $a = 5.69$ mm and $b = 2.845$ mm. A simple gap in an aluminum (6061-T6 alloy [16]) WR22 waveguide has been modeled using ANSYS HFSS, as shown in Fig. 2, where T is the waveguide wall thickness, and d is the gap between the two waveguide sections. The length L of each waveguide section is equal to 28.35 mm.

In Fig. 3, the IL and the RL of the structure shown in Fig. 2 are reported for different values of the waveguide wall thickness T when the waveguide gap d is equal to 100 μm.

As shown from the plots in Fig. 3, due to the power radiated through the gap aperture, the frequency response exhibits undesired transmission minima, which depend on the value of the waveguide wall thickness T. However, with a suitable choice of this value, it is possible to confine these minima outside the required band. In this case, for a gap of 100 μm, the optimal value of T is equal to 2.35 mm, which ensures a maximum IL of 0.17 dB, and a RL better than 28 dB over the operating bandwidth.

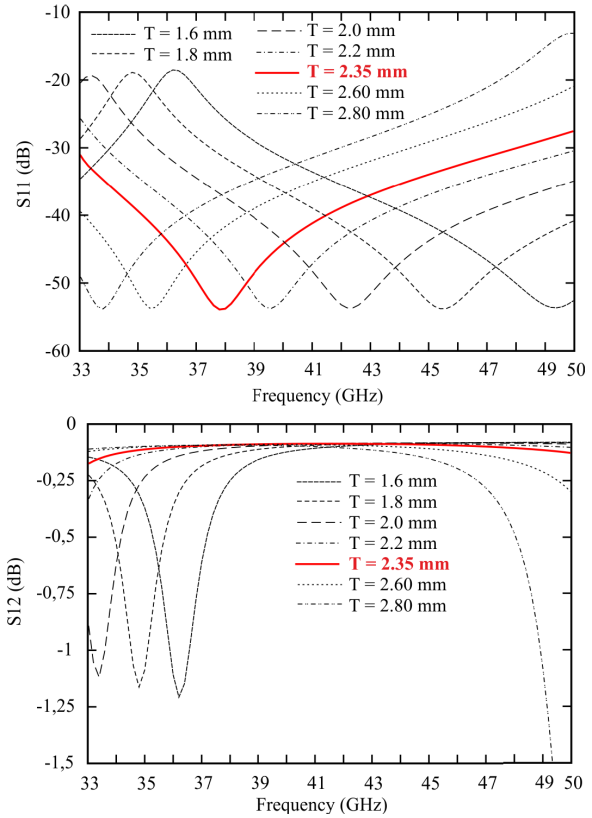

Fig. 3. Scattering parameters of the single-channel thermal isolator for different values of the waveguide wall thickness T ($d = 100$ μm).

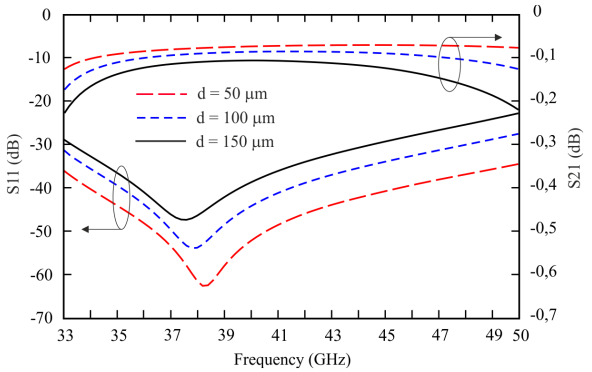

Fig. 4. Scattering parameters of the single-channel thermal isolator for different values of the gap d ($T = 2.35$ mm).

The selected $T = 2.35$ mm gives good results even for different values of the waveguide gap d, as shown in Fig. 4, wherein the scattering parameters of the thermal isolator are shown for d varying between 50 and 150 μm (which is the range of interest in our case).

The alignment of the two waveguide sections of a thermal isolator is always a crucial point to be accurately addressed in the design of the structure, especially in the Q-band and at higher frequency, wherein a high manufacturing accuracy is mandatory to achieve a good performance. Misalignment could occur due to several reasons, mainly realization tolerances and positioning of the component during the assembly of the receiver chain. Therefore, we need to be sure that a misalignment (at least) of the order of magnitude of the

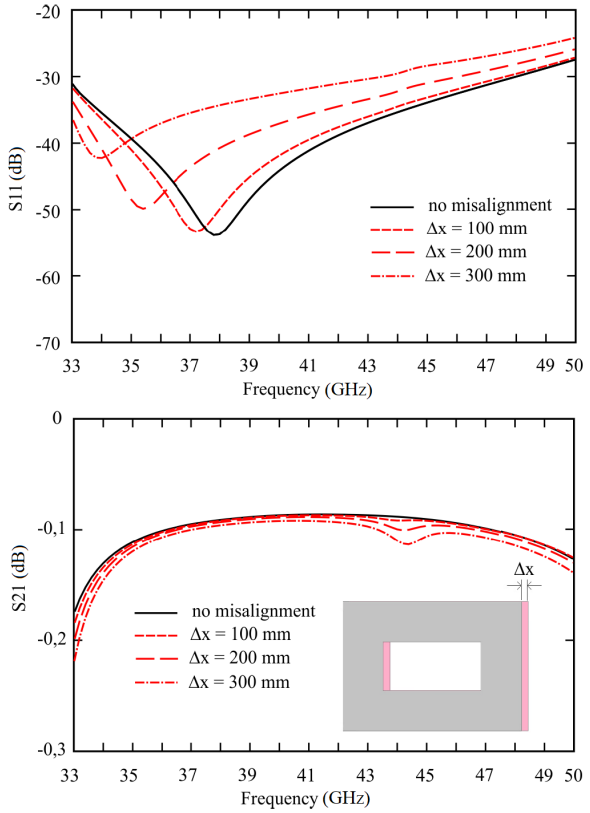

Fig. 5. Scattering parameters of the single-channel thermal isolator for different misalignments along x ($d = 100$ μm).

realization tolerances will not degrade neither the IL nor the RL.

In Figs. 5 and 6, a generic misalignment in the x- and y-directions (Δx and Δy, respectively) is considered. The value of the gap is $d = 100$ μm, but similar results can be observed for different values of d. The proposed configuration provides a good robustness even to a substantial misalignment of the two waveguide flanges: simulated results show that the RL is better than 24 dB in the worst case of $\Delta x = 300$ μm, whereas the IL varies in the range of 0.17–0.22 dB.

In Fig. 7, the effect of the rotation of the flanges is studied for $d = 100$ μm. A relative rotation up to 6° has been evaluated, which corresponds to a maximum displacement of $d_s = 290$ μm (see Fig. 7): in this case, the RL is not affected, whereas the IL is less than 0.28 dB.

Finally, in Fig. 8, the tilting of the flanges is investigated. The gap at the waveguide center is set to 100 μm and a tilting of 1.35° and 1° is applied, respectively, along the broad wall and narrow wall of the waveguide. A larger angle will cause the contact between the external edge of waveguide walls (i.e., with a spacing of less than 10 μm). However, this is unlikely to happen since the gap is controlled during assembly using metallic spacers, which are removed after screwing the G10 columns. The simulated RL is better than 26 dB and the IL is less than 0.17 dB.

Before discussing, in Section II-B, the design of the 3-channel thermal isolator, it is worth noting that substantially the same performance as described above can be achieved using a circular external profile of radius R instead of a rectangular one (as shown in Fig. 9).

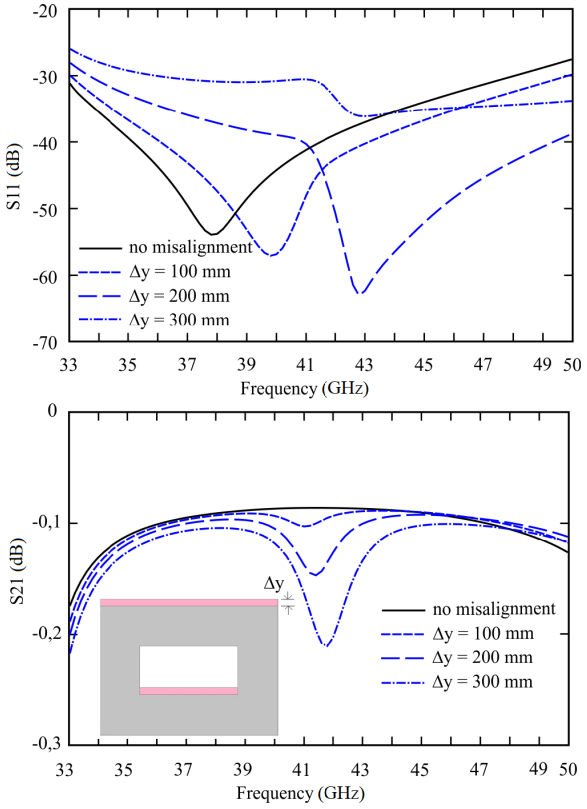

Fig. 6. Scattering parameters of the single-channel thermal isolator for different misalignments along y ($d = 100$ μm).

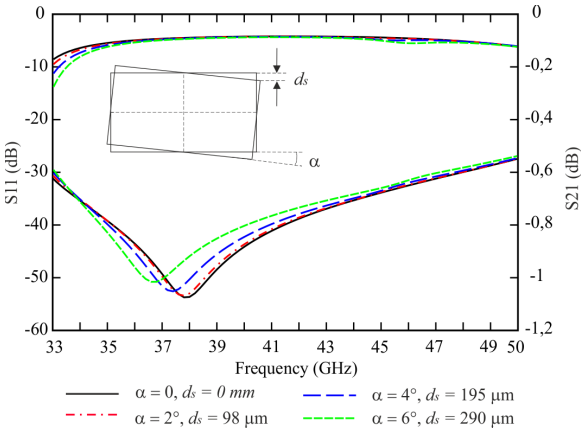

Fig. 7. Scattering parameters of the single-channel thermal isolator for a rotation of the flanges for $d = 100$ μm.

In this case, from HFSS simulations, we have found that the optimal R is equal to 3.8 mm. In this article, we have used the rectangular profile since it allows an easier and more accurate realization, based on the manufacturing technology available in our laboratory.

B. Design of the Three-Channel Waveguide Thermal Isolator

Three WR22 waveguide channels with proper wall thickness T (selected according to the design guidelines in Section II-A) are embedded in a metallic frame of aluminum. The proposed design is shown in Figs. 1 and 10.

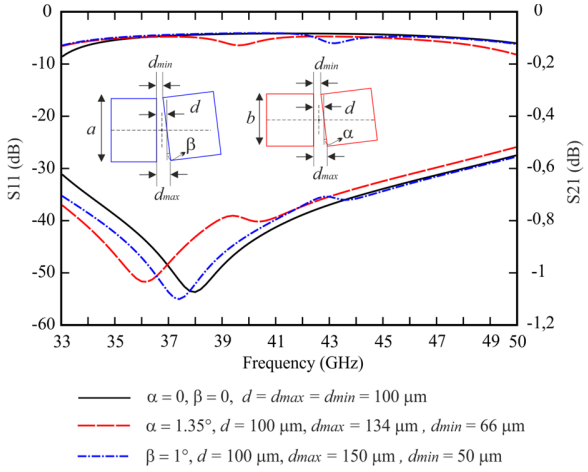

Fig. 8. Scattering parameters of the single-channel thermal isolator for a tilting of the flanges.

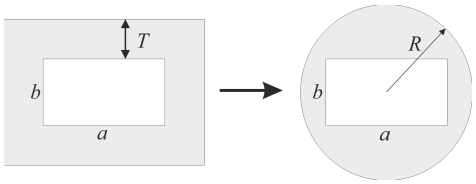

Fig. 9. WR22 waveguide flange with external circular profile.

The footprint of the component [Fig. 10(a)] is dictated by the connection to the Orthomode Transducer, which will be designed for the specific application. In this regard, the distance between the horizontal polarization channel and the vertical one (ports 1–2 and 3–4) has been fixed to I1 = 9.9 mm, whereas the distance between the two main channels and the third one, employed for the noise injection (ports 5–6), is dictated by the position of the noise generator and has been set to I2 = 26.8 mm.

Three G-10 fiberglass-epoxy flat columns have been used to sustain the two waveguide flanges of each module. The hexagonal shape of the external part of the flanges, with the G-10 columns placed at 120° along alternating faces of the hexagon (see Fig. 10), allows a high mechanical stability. The detailed geometry of the G-10 columns used in our case is shown in Fig. 11: their length is set to 47 mm (at room temperature, when $d = 100$ μm), whereas their thickness is equal to 2 mm.

High accuracy of the gap d can be achieved by placing metallic spacers between the flanges during assembly, whereas the alignment is obtained using two dowel pins.

It should be noted that particular attention has been paid to the selection of the length of the G-10 insulators since it determines the longitudinal dimension of the component, which should be reduced as much as possible (due to the limited space available inside the cryostat), but it also determines the thermal flow. The thermal performance of the proposed isolator is reported in Section III.

The above-mentioned design should be verified from the electromagnetic point of view to ensure that the behavior

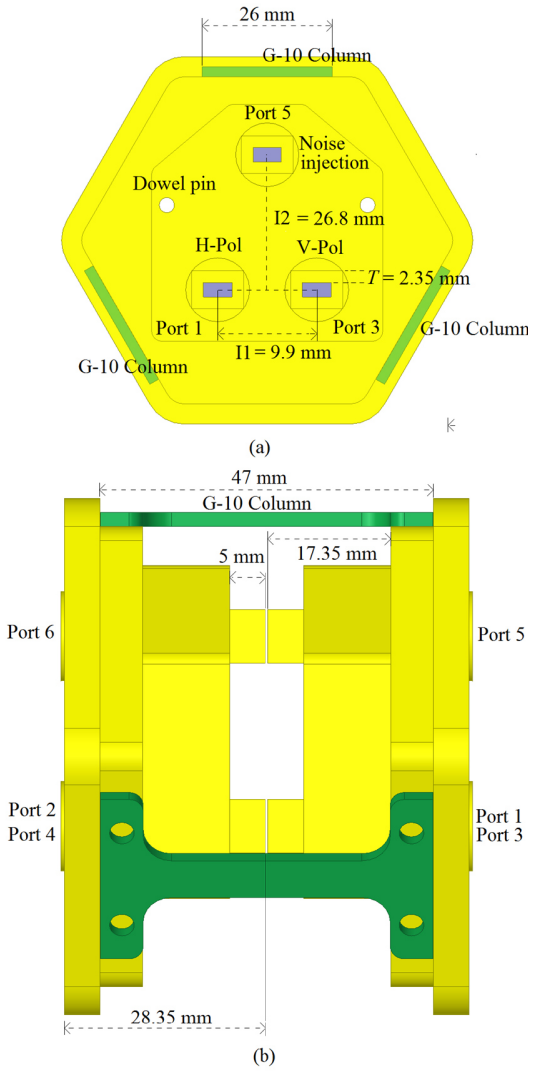

Fig. 10. Model of the thermal isolator. (a) Front view. (b) Side view.

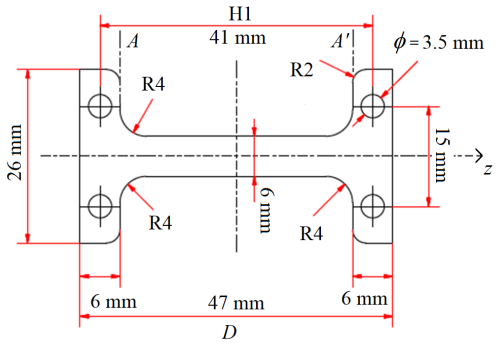

Fig. 11. Geometry of the G-10 fiberglass-epoxy flat column.

of the whole three-channel structure is consistent with the design guidelines reported in Section II. The waveguide wall thickness T is the design parameter used to optimize the electromagnetic performance of the isolator, and there is a 5-mm waveguide trunk of wall thickness T for each side of the thermal isolator outside the main block [see Fig. 10(b)]. In this way, as can be seen from the comparison in Fig. 12 (for $T = 2.35$ mm and $d = 100$ μm), we guarantee that

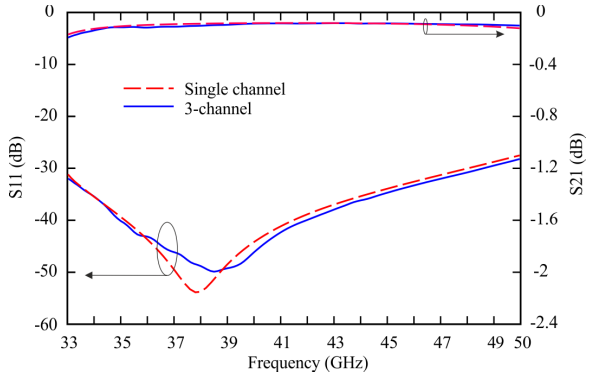

Fig. 12. Simulated comparison between the scattering parameters of the single-channel configuration in Fig. 2 and the three-channel module in Fig. 1, $T = 2.35$ mm, and $d = 100$ μm.

each channel of the proposed three-channel isolator exhibits virtually the same frequency response of the single-channel configuration. The same agreement as shown in Fig. 12 can be found for different values of the gap d and when the two flanges are misaligned.

Consequently, the design curves reported in Figs. 3–8 can be used also for the design of the three-channel isolator. As a further verification, the mutual coupling between different channels (i.e., $|S_{14}|$ and $|S_{16}|$) should be evaluated since it could degrade the performance of the receiver. From ANSYS HFSS simulations, we have found that it remains below -45 dB for different values of the waveguides gap d (50, 100, and 150 μm).

III. Thermal Characterization of the Isolator

Some of the components of the cryogenic receiver should operate at the temperature of 20 K; therefore, one flange of the thermal isolator is intended to be connected to 20 K, whereas the other one operates at room temperature (300 K).

First, the thermal properties of the isolator are investigated since they influence the power required to maintain the operating cryogenic temperature.

Second, it should be noted that the materials are subjected to thermal contraction when cooled from room temperature to cryogenic temperature [17]. This contraction could affect the electromagnetic design of the isolator mainly at millimeter wavelengths and has been discussed in Section III-B.

A. Evaluation of the Thermal Power

The maximum thermal flux allowed for a single module has been fixed to 150 mW by the design specification of the receiving system. Then, given the transverse section of the G-10 columns, equal to 6 mm $\times$ 2 mm (see Fig. 11), their length D should be such that the thermal flux across the single column is less than 50 mW.

Experimental measurement of the thermal resistance of the G-10 columns is not performed in this work. However, measured data of the thermal properties of the G-10 material are provided by the U.S. National Institute for Standards and Technology (NIST).

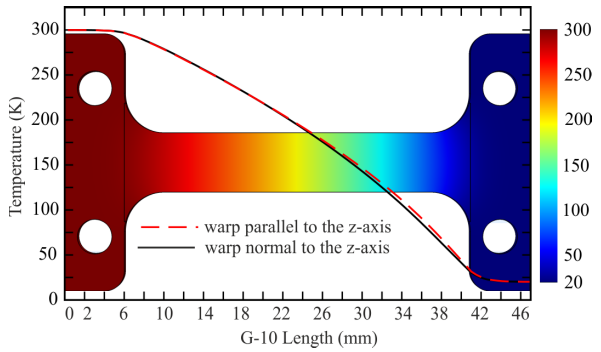

Fig. 13. Temperature distribution along the axis of the G-10 column computed with COMSOL Multiphysics. Continuous line: warp normal to the z-axis. Dashed line: warp parallel to the z-axis. The temperature diagram in the background is relative to case 2.

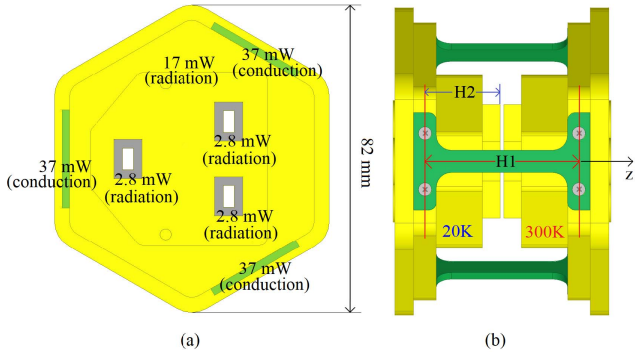

Fig. 14. (a) Section view of the thermal isolator with indication of the thermal flux. (b) Side view of the thermal isolator with an indication of the spacings subjected to contraction.

The thermal flux across a G-10 column has been computed by means of the commercial software COMSOL Multiphysics. This software requires setting the thermal and mechanical properties of a specific material to perform the computation of the thermal flux across a complex 3-D structure, which is modeled using the finite-element method. Therefore, the measured data of the thermal conductivity of the G-10, available from the NIST, have been set in the COMSOL interface to compute the thermal flux across the G-10 column, imposing the required boundary conditions (i.e., the temperature is set to 20 and 300 K, respectively, at the G-10 sections in direct contact with the two flanges).

Two different cases should be considered.

1) The direction of the G-10 column (z-axis in Fig. 11) is parallel to the warp direction of the material.
2) The direction of the G-10 column is perpendicular to the warp.

The thermal flux is 53 mW in case 1) and 37 mW in case 2). The temperature distribution along the G10 column in these cases is reported in Fig. 13.

The above results suggest that, to minimize the required refrigerating power, the G-10 columns should be manufactured with the warp normal to the z-axis.

Up until now, in the thermal evaluation, we have not considered the effect of the thermal radiation due to the surface (about 0.0041 m^2) of the flange at 300 K. This contribution can be computed by means of the Stefan–Boltzmann law for parallel surfaces [17], [18], using the emissivity of polished aluminum (usually in the range of 0.02–0.1) [18], [19]. Considering a conservative value of 0.1 for the emissivity of aluminum, we obtain a radiative thermal flux around 188 mW. This value can be reduced by about a factor of 11 [19] using a sheet of polyester superinsulation, composed of ten layers (e.g., type COOLCAT 2 by RUAG), to mask the surface of the cold flange facing its counterpart at 300 K. The result is a thermal flux of 17 mW. If needed, this value can be further reduced using a sheet of superinsulation with more layers.

However, the transverse surface of each waveguide wall in the region of the gap (about 6.2×10^{-5} m^2) cannot be masked by the sheet of polyester superinsulation, leading to a thermal load of about 2.8 mW for each channel.

In conclusion, the total estimated thermal flux for our component is about 136 mW [see Fig. 14(a)].

B. Evaluation of the Thermal Contraction

The waveguide flange connected to the cold end at 20 K and the G-10 columns are subjected to thermal contraction according to the thermal and mechanical properties of the aluminum alloy 6061-T6 and of the G-10 fiberglass epoxy. The linear expansions of these materials, available from the NIST, have been set in COMSOL Multiphysics to compute their contraction.

Three main effects should be considered [see Fig. 14(b)] as follows.

1) The contraction of the transverse section of the aluminum flange at 20 K.
2) The contraction in the longitudinal direction (z-axis) of the aluminum flange at 20 K, which should be applied to the spacing between the screws fixing the G-10 columns to the aluminum flange and the edge of the gap (H2 in Fig. 14).
3) The contraction in the longitudinal direction (z-axis) of the G-10 columns, which should be applied to the spacing between the screws fixing the G-10 to the aluminum flanges (H1 in Fig. 14).

The contraction of the transverse section of the aluminum flange at 20 K leads to a reduction of 24 μm of the waveguide width a, a reduction of 12 μm of the waveguide height b, and a reduction of 10 μm of the waveguide wall thickness T. From ANSYS HFSS simulations, we have found that such contractions correspond to a variation less than 0.02 dB for the IL and less than 0.6 dB for the RL. These variations do not affect the electromagnetic performance in the operating frequency range and can be neglected in the design procedure.

The contraction of the spacing H2 (Aluminum alloy 6061 T6), which is equal to 20.35 mm at room temperature, is about 82 μm.

Finally, the contraction of the spacing H1, which is equal to 41 mm at room temperature (Fig. 11) and is relative to the G-10 column fabricated with the warp normal to the z-axis (according to Section III-A), is about 145 μm.

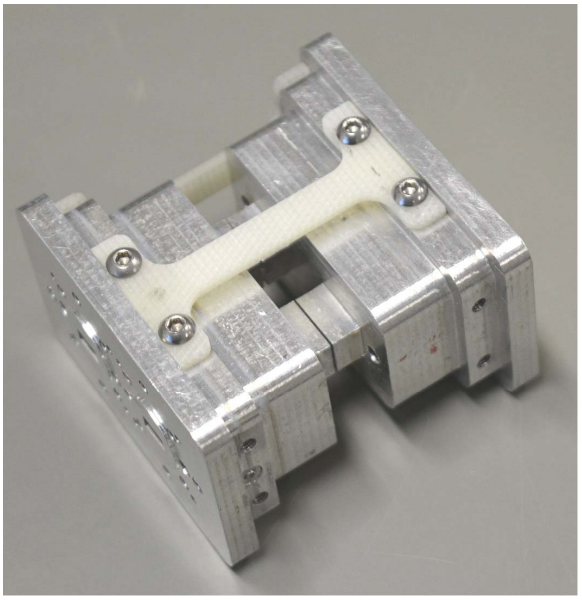

Fig. 15. Photograph of the realized prototype of the two-channel thermal isolator.

Consequently, the gap d reduces by about 60 μm under operating conditions. This should be taken into account during the assembly of the component at room temperature.

IV. Experimental Verification

A simplified prototype of the thermal isolator (see Fig. 15) has been manufactured to assess the proposed design. In this case, the channel for the injection of the noise source is not present. However, this will not change the electromagnetic performance of the two main channels because, as remarked in Section II-B, the coupling between different channels is negligible.

The calibration procedure of the vector network analyzer (VNA) (model Rohde & Schwarz ZVA67) for the direct measurement of the scattering parameters under actual operating conditions could be quite complicated because the waveguide sections of the thermal isolator should be at different temperatures (i.e., 300 and 20 K). For this reason, the prototype shown in Fig. 16 has been measured with both the waveguide sections at room temperature.

As pointed out in Section III, the thermal contraction occurring at cryogenic temperature can be easily accounted for during the design procedure, paying attention to avoid the contact between the two waveguide flanges when one of them is cooled at cryogenic temperature.

In Fig. 16, the frequency response of one channel of the prototype shown in Fig. 15 is reported for a gap $d = 50$ and 100 μm, and a waveguide wall thickness $T = 2.35$ mm (the plots for the two channels virtually overlap). The value of the gap has been set using 50- and 100-μm metallic spacers during assembly and has been subsequently verified by a precision measurement using a microscope.

The agreement between measurement and simulation (ANSYS HFSS) is good, showing a measured IL less than 0.3 dB (0.22 and 0.28 dB, respectively, for $d = 50$ μm and $d = 100$ μm) and an RL higher than 30 dB over the Q-band. The measured mutual coupling S_{41} between the two channels is below -50 dB [see Fig. 16(c)].

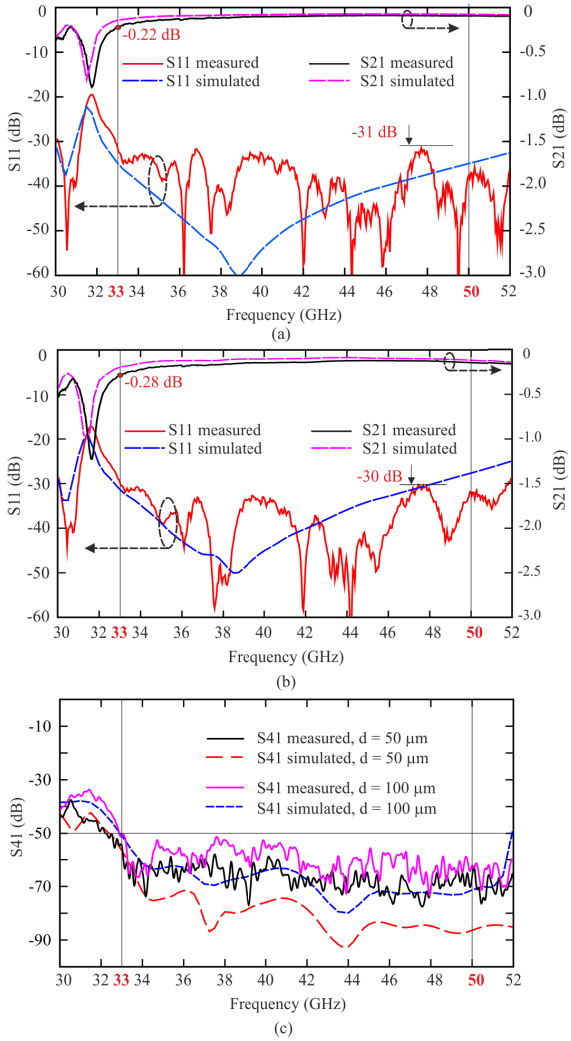

Fig. 16. Comparison between simulated and measured results for the prototype in Fig. 15. (a) S_{11} and S_{21} for $d = 50$ μm. (b) S_{11} and S_{21} for $d = 100$ μm. (c) S_{41} for $d = 50$ and 100 μm.

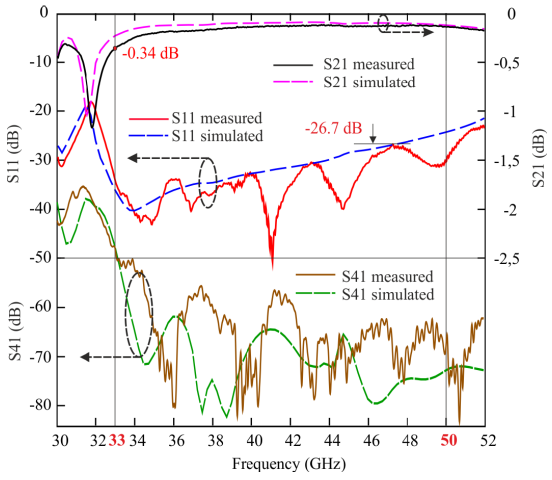

Fig. 17. Comparison between simulated and measured results for the prototype in Fig. 15: $d = 100$ μm, $\Delta x = 300$ μm, and $\Delta y = 0$.

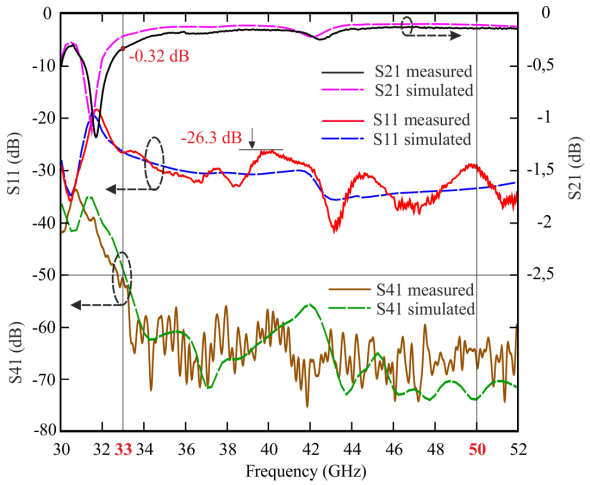

Fig. 18. Comparison between simulated and measured results for the prototype in Fig. 15: $d = 100\ \mu$m, $\Delta x = 0\ \mu$m, and $\Delta y = 300\ \mu$m.

Finally, a misalignment along x or along y has been generated with suitable metallic spacers during the assembly of the prototype. The following configurations have been considered.

1) $\Delta x = 300\ \mu$m, $\Delta y = 0$, and $d = 100\ \mu$m.
2) $\Delta y = 300\ \mu$m, $\Delta x = 0$, and $d = 100\ \mu$m.

The above spacings have been verified by measurement using a microscope. The measured scattering parameters of these configurations are reported in Figs. 17 and 18 showing an IL less than 0.34 dB, an RL better than 26 dB, and a mutual coupling S_{41} below -50 dB.

Finally, it should be noted that, since the conductivity of the aluminum increases at cryogenic temperature [17], [20], the IL reduces, compared to the values measured at room temperature when one of the two waveguide flanges is cooled at 20 K.

V. Conclusion

A new rectangular waveguide thermal isolator for high-performance cryogenic receivers has been designed and characterized. It is a common opinion among researchers that a thermal isolator consisting of a simple gap in a standard waveguide is not able to provide the required electromagnetic performance due to in-band transmission minima. However, to the best of our knowledge, probably, the easiest solution to this problem has not been investigated yet: it consists in moving the transmission minima outside the operating band by a proper selection of the waveguide wall thickness. In our work, this strategy has been successfully applied to the design of a performing thermal isolator for the Q-band cryogenic receiver of the SRT.

Acknowledgment

The authors would like to thank A. Saba, G. Mazzarella, J. Roda, and S. Mariotti for their useful advice.

References

[1] T. Wilson, K. Rohlfs, and S. Huettemeister, *Tools of Radio Astronomy* (Astronomy and Astrophysics Library), 6th ed. Berlin, Germany: Springer, 2014.
[2] J. D. Kraus, *Radio Astronomy*, 2nd ed. New York, NY, USA: McGraw-Hill, 1986.
[3] P. Bolli *et al.*, "Sardinia Radio Telescope: General description, technical commissioning and first light," *J. Astron. Instrum.*, vol. 4, nos. 3–4, 2015, Art. no. 1550008.
[4] M. Davidovitz, "A low-loss thermal isolator for waveguides and coaxial transmission lines," *IEEE Microw. Guided Wave Lett.*, vol. 6, no. 1, pp. 25–27, Jan. 1996.
[5] J. L. Hesler, A. R. Kerr, and N. Horner, "A broadband waveguide thermal isolator," in *Proc. 14th Int. Symp. Space THz Technol.*, Tucson, AZ, USA, Apr. 2003, pp. 148–154.
[6] T. Kawaguchi *et al.*, "High-sensitivity HTS receiver module with hermetic thermal insulation waveguides," in *Proc. 43rd Eur. Microw. Conf.*, Nurenberg, Germany, Oct. 2013, pp. 955–958.
[7] G. Valente, G. Montisci, T. Pisanu, A. Navarrini, P. Marongiu, and G. A. Casula, "A compact L-band orthomode transducer for radio astronomical receivers at cryogenic temperature," *IEEE Trans. Microw. Theory Techn.*, vol. 63, no. 10, pp. 3218–3227, Oct. 2015.
[8] G. Valente *et al.*, "Status of the radio receiver system of the Sardina Radio Telescope," *Proc. SPIE*, vol. 9914, Jul. 2016, Art. no. 991425, doi: 10.1117/12.2232880.
[9] E. Flamini *et al.*, "Deep space communication service provided by sardinia deep space antenna—SDSA: Program status and cababilities," presented at the 68th Int. Astron. Congr., Adelaide, SA, Australia, Sep. 2017, Paper IAC-17.B2.8-GTS.3.4.
[10] G. Muntoni *et al.*, "Space debris detection in low earth orbit with the Sardinia Radio Telescope," *Electronics*, vol. 6, no. 3, p. 59, Aug. 2017.
[11] G. Muntoni *et al.*, "A space debris-dedicated channel for the P-band receiver of the Sardinia Radio Telescope: A detailed description and characterization," *IEEE Antennas Propag. Mag.*, to be published.
[12] N. Skou, *Microwave Radiometer Systems: Design and Analysis*, 2nd ed. Norwood, MA, USA: Artech House, 1989.
[13] G. Valente, G. Montisci, and S. Mariotti, "High-performance microstrip directional coupler for radio-astronomical receivers at cryogenic temperature," *Electron. Lett.*, vol. 50, no. 6, pp. 449–451, Mar. 2014.
[14] M. B. Kasen, G. R. MacDonald, D. H. Beekman, Jr., and R. E. Schramm, "Mechanical, electrical, and thermal characterization of G-10CR and G-11CR glass-cloth/epoxy laminates between room temperature and 4 K," in *Advances in Cryogenic Engineering Materials*, A. F. Clark and R. P. Reed, Eds. Boston, MA, USA: Springer, 1980, pp. 235–244.
[15] G. L. Ragan, *Microwave Transmission Circuits*, 1st ed. New York, NY, USA: McGraw-Hill, 1948.
[16] J. R. Davis, *Aluminum and Aluminum Alloys*, 5th ed. Cleveland, OH, USA: ASM International, 2007.
[17] J. G. Weisend, II, Ed., *The Handbook of Cryogenic Engineering*, 1st ed. New York, NY, USA: Taylor & Francis, 1998.
[18] W. M. Rohsenow, J. R. Hartnett, and Y. I. Cho, *Handbook of Heat Transfer*, 3rd ed. New York, NY, USA: McGraw-Hill, 1998.
[19] S. White, R. Simon, and G. Petencin, "On radiation loading in cryogenic dewars and emissivity measurements for radiation shield materials," Nat. Radio Astron. Observatory, Charlottesville, VA, USA, Electron. Division Internal Rep. 323, Apr. 2011.
[20] S. Weinreb, "Cryogenic performance of microwave terminations, attenuators, absorbers, and coaxial cable," Nat. Radio Astron. Observatory, Charlottesville, WV, USA, Electron. Division Internal Rep. 223, Jan. 1982.

Giorgio Montisci (M'08–SM'19) received the M.S. degree in electronic engineering and the Ph.D. degree in electronic engineering and computer science from the University of Cagliari, Cagliari, Italy, in 1997 and 2000, respectively.

Since November 2015, he has been an Associate Professor of electromagnetic fields with the University of Cagliari, teaching courses in electromagnetics and microwave engineering. He has authored or coauthored about 70 articles in international journals. His current research interests include the analysis and design of waveguide slot arrays, RFID antennas, wearable antennas, numerical methods in electromagnetics, and microwave circuits and systems.

Dr. Montisci is an Associate Editor of IEEE Access and *IET Microwaves, Antennas and Propagation* and an Academic Editor of the *International Journal of Antennas and Propagation*.

Giuseppe Valente received the M.S. degree in electronic engineering and the Ph.D. degree in electronic engineering and computer science from the University of Cagliari, Cagliari, Italy, in 2007 and 2016, respectively.

From 2009 to 2016, he was with the National Institute for Astrophysics (INAF), Cagliari Astronomy Observatory, Cagliari, where he was involved in the development of the receivers for Sardinia Radio Telescope (SRT). In 2016, he joined the Italian Space Agency (ASI), Rome, Italy. His current research interests include the electromagnetic design of passive and active devices for microwave and millimeter-wave receivers and instrumentation.

Giacomo Muntoni received the M.S. degree in telecommunication engineering and the Ph.D. degree in electronic engineering and computer science from the University of Cagliari, Cagliari, Italy, in 2015 and 2019, respectively.

His current research interests include the design and characterization of antennas for biomedical applications, radar systems for space debris monitoring, and microwave components.

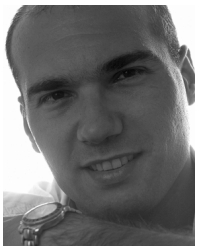

Pasqualino Marongiu received the Diploma of DSE-Industrial Engineer degree in mechanics from the High School of Sassari, Sassari, Italy, in 1995.

For 10 years, he was with private companies responsible for mechanical production and quality control. Since 2009, he has been with the National Institute for Astrophysics (INAF), Cagliari Astronomy Observatory, Cagliari, Italy, where he is involved in the development of the receivers and mechanical design for the Sardinia Radio Telescope (SRT).

Tonino Pisanu received the M.S. degree in physics from the University of Cagliari, Cagliari, Italy, in 1995.

In 2001, he joined the National Institute for Astrophysics (INAF), Cagliari Astronomy Observatory, Cagliari. His current research interests include the analysis and design of microwave components for radio astronomy applications and research and development of noncontact measuring systems for characterizing and correcting the optical shape and mechanical configuration of big antenna systems.